SUPPRESSION OF FAN NOISE OF HIGH CIRCUMFERENTIAL MODE USING OPTIMIZED DUCT WALL PROPERTIES

Lixi HUANG

Department of Mechanical Engineering, The University of Hong Kong, Pokfulam Road, Hong Kong SAR, China

SUMMARY

Sound absorption by a duct lining or an impedance wall is most effective in the medium frequency range. The attenuation spectrum tails off at both low- and high-frequency extremes. This study investigates, theoretically, the absorption of high frequency, high circumferential order rotor noise by a microperforated panel with an axially distributed cavity depth, porosity and aperture diameter. The wave equation is solved in the frequency domain with the Chebyshev collocation method. It is shown that a passive absorber with such an optimized property can greatly enhance the absorption performance. In a typical example given, the optimization gives more than 4 dB extra attenuation per unit distance equal to the rotor radius.

NOMENCLATURE

A_{mn}	modal amplitude of point source at $r = r_s$
c_0	speed of sound in air
d	aperture diameter in micro-perforated panel
$f = f^* r^*_{tip}/c^*_0$	frequency normalized by c^*_0/r^*_{tip} (asterisks indicate dimensional)
f_{12}	12 discrete frequencies defined in Eq. (17)
h_c	cavity depth behind micro-perforated panel or interface at $r = r_{tip}$
$i = \sqrt{-1}$	imaginary number
IL	insertion loss in dB
I_r, I_x	radial and axial sound intensity
I_{r1}	radial intensity normalized by nominal local sound energy flux, Eq. (14)
j	integer (index)
k, k_{mn}, k_{xmn}	wavenumber, modal wavenumber and axial wavenumber
K	ratio of aperture diameter to boundary layer thickness, Eq. (3)

L_r	sound attenuation in dB per unit distance equal to rotor tip radius r_{tip}
L_U, L_M, L_D	upstream, middle and downstream domain lengths
$m, n, \partial/\partial n$	indices of circumferential and radial modes, normal derivative
N_r	number of Gauss-Lobatto mesh segments
$p = -\rho_0 \partial\phi/\partial t$	sound pressure and its relation with velocity potential ϕ
r, r_{hub}, r_{tip}	radius, hub and tip radii
R	resistance component of impedance Z
r_s	point source radius
SPL_n	sound pressure level for the nth radial mode
t	time (normalized by r^*_{tip}/c^*_0)
TL	transmission loss in dB
t_p	panel thickness
$W_{in,ref,abs,ex}$	sound power at incidence, reflection, absorption and exit
Z	acoustic impedance, $p/(\rho_0 c_0 \partial\phi/\partial r)$

α, β	absorption and reflection coefficients of sound
η	air viscosity
ϕ	velocity potential
$\omega = 2\pi f$	angular velocity
ρ_0	air density
μ	number of terms in the Chebyshev series for the distributed wall property
σ	panel perforation ratio (porosity)
θ	angular coordinate
Ξ	pseudo-derivative operator, Eq. (7)

Subscripts - 0: air; c: cavity; mpp: microperforated panel; LE: leading edge

Superscripts - *: dimensional variables; (in): incident wave; (s): scattered

1. INTRODUCTION

Passive control is a preferred engineering solution for many noise problems including fan noise. This study explores the use of distributed duct wall property to control the high frequency fan noise with high circumferential mode index. Duct noise control finds many applications in engineering, ranging from central ventilation noise in buildings, engine inlet and exhaust noise in turbomachines (Blake 1986), motor vehicles (Munjal et al 2006), as well as in aircraft engines (Hubbard 1995). In an engine, the main aerodynamic noise source is often the interaction between rotor blades and stators, for which a spinning pressure pattern (Tyler & Sofrin 1962) causes dipole noise to radiate to the two sides of the blades. With a special interest in aeroengine noise, we focus on circular ducts with a high order of circumferential mode, m, while the potentially strong effect of high-speed flow is temporarily set aside. The question we ask is whether a distributed passive wall property can absorb significantly more noise than a uniform wall property over a reasonably broad frequency band and with multiple radial modes. For the typical example given in this preliminary study, which has an absorber length equal to the casing diameter, distributed wall property gives an 8.5 dB improvement from the uniform wall property which is itself optimized.

The wall in the present study is modelled as a locally reactive impedance consisting of micro-perforated panel (MPP) backed by a cavity. Alternatively, we also consider replacing the MPP by an interface impedance with components of mass, spring and damper. These generic components have constant properties independent of frequency. This contrasts with active control schemes (Thomas et al 1994, Nauhaus et al 2003) in which equivalent wall properties are functions of frequency and may vary from time to time. In active control, each duct acoustics mode requires at least one independent actuator, or control channel. Similarly, we increase the number of independent passive wall properties when the number of radial modes to be attenuated increases. Note that the total absorber length is fixed for a given problem.

In a two-dimensional planar duct, mode n has a wavelength equal to $n/2$ times the duct height. When the source frequency just reaches a cut-on frequency, sound is actually bouncing between the two walls. The situation is similar in circular ducts but with a radial wave distribution different from its planar counterpart. In addition, there is a circumferential mode number, denoted here as m, which is determined by the source characteristics. The mode of m=n=0 corresponds to the plane wave. In our study, we fix m as 16, which is a typical value in aero-engine applications (Rienstra & Eversman 2001, Sun et al 2008).

At a high frequency, many cut-on modes appear and it is known that the low-order cut-on modes are more difficult to control. In aircraft applications, the out-of-duct radiation of these low-order modes may be focused in lobes that are closely aligned with the flight direction. It is thus less of a concern for flight certification. Nevertheless, noise control at all modes would help reduce acoustic fatigue and is always desirable. The excitation of a particular radial mode depends on the source distribution. If the source is taken as a concentrated point, low-order modes are excited more strongly when the source is closer to the outer radius. In this study, we place a point source at a radial position equal to 88% of the outer radius, which is considered to be a typical peak position for the aerodynamic loading along a blade span.

The approach taken by this study is numerical optimization for the duct wall impedance distribution. A very accurate numerical scheme of Chebyshev collocation is adopted. Details are given in Sec. 2 with method validation. Sec. 3 presents the numerical results for single frequency while Sec. 4 extends the results to broadband frequency. Conclusions are given in Sec. 5. The work presented below consists of two parts, one using the conceptual wall resistance (Figure 2) and the other is based on the practical implementation of microperforated panel (Figures 3-5). The former part was presented at ICSV 18 (Rio de Janeiro, 10-14 July 2011).

2. NUMERICAL METHOD AND ITS VALIDATION

As shown in Figure 1, we consider an infinite-length annular duct of outer (tip) radius r_{tip}^* and inner (hub) radius r_{hub}^*. Spinning pressure pattern creates such noise that it can be represented by a point source at radius $r^* = r_s^*$ with a circumferential dependence of $\exp(im\theta)$, where m is the circumferential modal index and θ is the angular coordinate. The speed of sound is c_0^* and the frequency is f^*. Before proceeding to formulation, all variables are normalized by using r_{tip}^* as the length scale, r_{tip}^*/c_0^* as the time scale, and the undisturbed air density ρ_0^* as the density scale. All variables with superscript asterisks are dimensional, and the removal of such superscript implies the dimensionless version of the same variable. For example, dimensionless frequency is defined as $f = f^* r_{tip}^*/c_0^*$ and a typical value of interest is f=(4000Hz)(0.5m)/(340m/s)= 5.88. We choose f=6 for most examples.

The configuration shown in Figure 1 has an absorber of dimensionless length L_M sandwiched in an

otherwise infinite annular passage formed between the radii of r_{hub} and $r_{tip}=1$. The absorber has a locally reactive impedance with a cavity of distributed depth $h_c(x)$, and a face impedance which can be either a microperforated panel (MPP) or a generic dynamic element. Since the cavity already has stiffness and air mass, the most useful generic element would be a frequency-independent resistance, denoted by R. The total acoustic impedance seen at $r=r_{tip}=1$ is written as

$$Z=\left.\frac{p^*}{\rho_{air}^* c_0^* \partial\phi^*/\partial r^*}\right|_{r_{tip}} = \frac{p}{\partial\phi/\partial r} = Z_{cavity} + \underbrace{Z_{face}}_{=Z_{mpp} \text{ or } R}, \quad Z_{cavity}=\frac{\rho_c c_c}{i\tan k_c h_c}, \tag{1}$$

where $\omega=2\pi f$ is the angular frequency, which is also identical to the dimensionless wavenumber $k=\omega^* r_{tip}^*/c_0^*$, ϕ is the velocity potential related to the sound pressure via $p=-\partial\phi/\partial t=-i\omega\phi$ with a time dependence of $e^{i\omega t}$. Here, $\rho_c, c_c,$ and k_c are, respectively, the fluid density, speed of sound and wavenumber in the cavity, which can be different from that of air, such as a filling by fibrous sound absorption material. For most examples given, however, air is assumed, hence $\rho_c=c_c=1, k_c=k$.

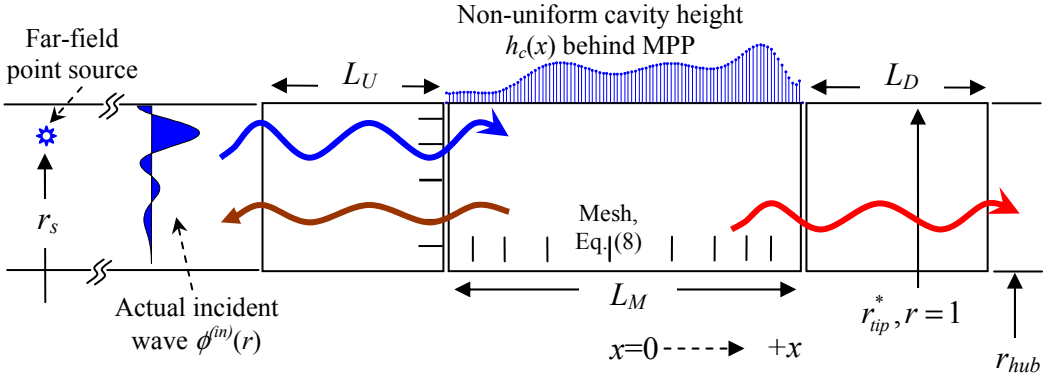

Figure 1: The theoretical and numerical configurations. A far-left point source introduces a packet of propagating incident waves, $\phi^{(in)}(r)$, which is scattered by an absorber segment of length L_M with distributed cavity depth $h_c(x)$ and perhaps an MPP with distributed perforation ratio and aperture diameter. The computational domain is truncated at a length of L_U in the upstream, and L_D in the downstream of the absorber. The non-uniform axial and radial Gauss Lobatto grids are also illustrated for the middle domain of length L_M.

If an MPP is used at $r=r_{tip}$, the surface-averaged panel impedance is (Maa 1992),

$$Z_{mpp}=\sigma^{-1}\left[32\frac{\eta t_p}{d^2}\sqrt{1+K/32}+\sqrt{\frac{k\eta}{2}}+ikt_p\left(1+\frac{1}{\sqrt{9+K^2/2}}\right)+i\,0.85kd\right], \tag{2}$$

where d, t_p and σ are aperture diameter, panel thickness and porosity, respectively, and

$$\eta=\frac{\eta^*}{\rho_0^* c_0^* r_{tip}^*}, \quad K=\frac{d}{2}\sqrt{\frac{k}{\eta}} \tag{3}$$

are the dimensionless viscosity and ratio of aperture diameter to the boundary layer, respectively.

On a real rotating blade, sound sources are mainly dipole in nature and waves propagate in both upstream and downstream directions. Complex reflection and interference pattern exists in a real passage. To focus on absorber optimization using wall impedance, we consider an elementary

source model. Imagine that a point source exists in a far upstream location at a radial position of $r=r_s$, the radiated wave may be separated into propagating (cut-on) and non-propagating (cut-off) modes in a rigid-wall duct. The former is considered as the given incident wave from the far left, which is then scattered by the finite absorber giving reflected and transmitted waves.

The modes take the form of $e^{-ik_{xmn}x}\phi_{mn}(r)$, where $k_{xmn}=\sqrt{k^2-k_{mn}^2}$ is the axial wavenumber corresponding to each radial modal wavenumber k_{mn}. The modes are the non-trivial solutions to the eigen-value equation with rigid-wall boundary conditions:

$$\left(\partial_{rr}^2+r^{-1}\partial_r-m^2r^{-2}\right)\phi_{mn}=-k_{mn}^2\phi_{mn},\quad \partial_r\phi_{mn}\big|_{r=r_{hub}}=0,\quad \partial_r\phi_{mn}\big|_{r=1}=0. \tag{4}$$

A point source of unit strength is expanded as

$$\delta(r-r_s)=\sum_{n=1}^{\infty}A_{mn}^{(in)}\phi_{mn},\quad A_{mn}^{(in)}=\frac{\int_{r_{hub}}^1\phi_{mn}\delta(r-r_s)rdr}{\int_{r_{hub}}^1\phi_{mn}^2rdr}=\frac{r_s\phi_{mn}(r_s)}{\int_{r_{hub}}^1\phi_{mn}^2rdr} \tag{5}$$

with superscript '*in*' signifying 'incidence'. The actual incident wave consists of all the propagating modes satisfying $k_{mn}\le k$, hence

$$\phi^{(in)}(r)=\sum_{k_{mn}\le k}A_{mn}^{(in)}e^{-ik_{xmn}x}\phi_{mn}(r). \tag{6}$$

An example of incident wave packet $\phi^{(in)}$ is shown in the left-hand side of Figure 1 with $r_s=0.88$.

As shown in Figure 1, x=0 is placed at the centre of the absorber, and the numerical solution is sought in the domain truncated at a distance of L_U, L_D from the two edges of $|x|=L_M/2$, respectively. The method of Chebyshev collocation is used in conjunction with an out-going wave condition for the scattered sounds at the domain boundaries of $x=-L_M/2-L_U, L_M/2+L_D$. Details of the numerical method is described in (Huang 2008) for a similar two-dimensional problem in Cartesian coordinates. Here, the problem is posed in the cylindrical coordinates, with the Helmholtz equation and the associated out-going wave condition derived from the following pseudo-derivative operator Ξ:

$$\left[\partial_{xx}+\partial_{rr}+r^{-1}\partial_r+\left(k^2-m^2r^{-2}\right)\right]\phi=0,\quad (\partial/\partial n+i\Xi)\phi^{(s)}=0,\quad \Xi=\sqrt{k^2-\partial_r^2-r^{-1}\partial_r-m^2/r^2}\ . \tag{7}$$

The boundary condition is applied on the scattered field, $\phi^{(s)}=\phi-\phi^{(in)}$. Here, n in $\partial/\partial n$ is the outward normal on the boundary. The radial derivative operator ∂_r is represented by the Chebyshev derivative matrix, and Ξ is implemented numerically by matrix square-root through eigen-value decomposition (diagonalization) of matrix (Huang 2008). The choice of the individual eigen-value square-root is such that the waves propagating away from the scatterer are retained. Note that the rigid-wall boundary conditions of $\partial\phi/\partial r=0$ at $r=r_{hub}$ and $r=1$ are embedded in the derivative matrix by replacing the velocity potential on the walls by those at the inner grid points. As a test of accuracy, A point source at $r_s=0.88$ is launched at frequency $f=6$ with 5 cut-on modes. The magnitudes of error at the downstream exit are 6.1×10^{-14}, 1.5×10^{-14}, 1.2×10^{-13}, 5.8×10^{-13} and 5.4×10^{-12} for the five modes, respectively. Similar high accuracy was achieved for the planar waves in (Huang 2008), which was also compared favourably with a perfectly matched layer technique (Singer & Turkel 2004). However, the latter has the advantage of being easier to use in localized numerical schemes while our scheme is more suitable for idealized models with moderate

computational domain and where high accuracy is desirable. The Gauss-Lobatto grid (Boyd 2001) used,

$$r_j = r_{hub} + (1 - r_{hub})\left[1 - \cos(\pi j / N_r)\right]/2, \quad j = 0, 2, \cdots, N_r, \tag{8}$$

is also illustrated in Figure 1 (labeled as 'mesh'), and the grid density used in the axial direction is the same as that in the radial direction. The following set of geometric parameters is used in the accuracy test, and these will also be considered as the "default" values in the subsequent examples unless otherwise specified,

$$r_{hub} = 0.3, \quad r_s = 0.88, \quad N_r = 30, \quad L_U = L_D = 1, \quad L_M = 2, \quad h_c = 0.03. \tag{9}$$

The typical frequency used is $f = 6$ but broad frequency band is considered in Sec. 4.

3. WALL IMPEDANCE OPTIMIZATION FOR SINGLE FREQUENCY

Before optimizing the wall impedance, we study the modal behaviour of lined duct as well as the performance of sound absorption by a uniform segment of absorber which will be used as a basis for comparison with distributed wall impedance. First, the upper rigid wall is replaced by the following impedance condition at $r = 1$ as follows,

$$\left(\partial\phi/\partial r + ikZ^{-1}\phi\right)_{r=1} = 0. \tag{10}$$

The eigen-value problem is then solved in the same way as the case for the rigid walls but all modes are expected to decay with axial distance. The mode with the lowest decay rate is the main concern. So, a logarithmic attenuation rate per unit axial distance equal to the tip radius, L_r, is defined below for this mode,

$$L_r = 20\log_{10}\left[\exp\left(-\mathrm{Im}\left(k_{xmn'}\right)\right)_{\min}\right] = 8.686\left[\mathrm{Im}\left(-k_{xmn'}\right)\right]_{\min} \ \mathrm{dB}. \tag{11}$$

The modal index is here denoted by *n'* and the modal distribution $\phi_{mn'}(r)$ is expected to be similar to the rigid-wall mode of $n = n'$ when the wall impedance is only slightly different from a rigid wall. In general, however, each decaying mode *n'* consists of all rigid-wall modes and the 'cut-on' mode can only be loosely defined as the ones whose attenuation rate is very small.

Figure 2(a) shows the result of modal calculation with a cavity depth fixed at $h_c = 0.03$ and the frequency fixed at $f = 6$, while the resistance R varies. A peak value of $L_r = 10.43$ dB is obtained for $R = 2.15$. Attenuation vanishes towards $R \to 0$ as there is no damping, and it does so again when $R \to \infty$ as the wall becomes effectively rigid. Figure 2(b) shows the complex, least attenuating mode, which can be expanded as a combination of rigid-wall modes with the first five modes having the amplitudes of 1.173, 1.081, 0.355, 0.194 and 0.128. When both cavity depth h_c and resistance R are allowed to vary, a higher value of L_r can be obtained for any specific frequency. The optimal absorber parameters are shown as functions of frequency in Figure 2(c) using a twin set of coordinate labels. Higher resistance and shallower cavity are required for higher frequency. The corresponding optimal L_r is shown in Figure 2(d). Notice that the value of L_r shoots up as frequency goes below 4.5 or so, and this actually signifies the cut-on of the relevant rigid-wall modes which are now all attenuated. For frequencies above about 6, the optimal L_r goes below around 10 dB, which implies that these "cut-on" modes are difficult to attenuate.

When a finite absorber segment is used, sound is partly reflected, partly transmitted, and the bulk sound power is hopefully absorbed. Time-mean sound energy flux is obtained by integrating the

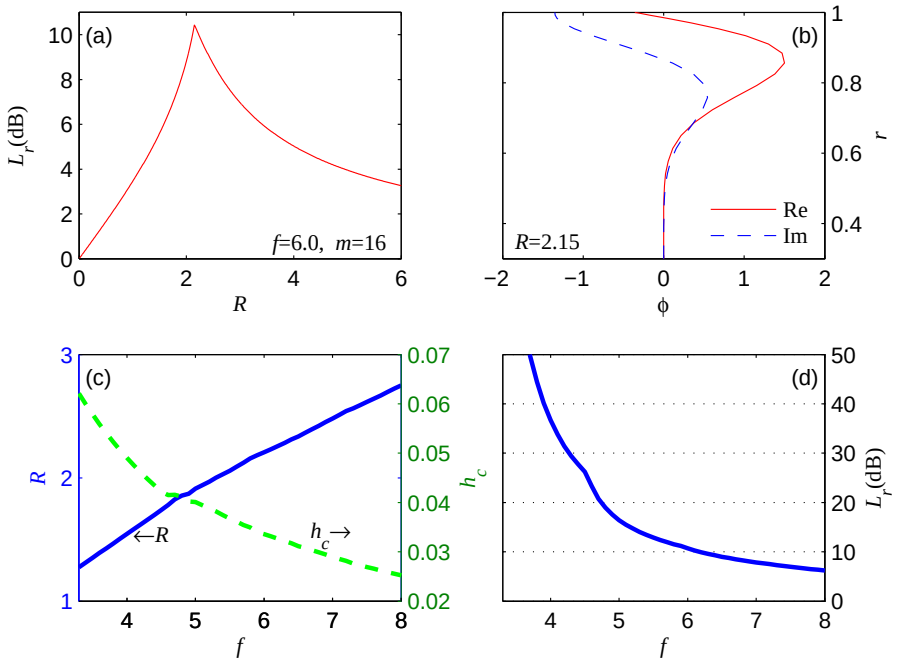

Figure 2: Optimization for the uniform wall impedance for m=16. (a) Attenuation L_r as a function of wall resistance R for h_c=0.03. (b) The least attenuating radial mode for the peak condition in (a) with R=2.15. (c) Optimal resistance R (see the left coordinate) and cavity depth h_c (right coordinate) for each frequency. (d) Variation of the optimal attenuation L_r with respect to frequency corresponding to the parameters in (c).

axial intensity flux I_x while sound absorption is obtained by integrating the radial intensity,

$$I_x(r)=\frac{1}{2}\mathrm{Re}\left(p\left(\partial\phi/\partial x\right)^*\right), W_x=\int_{r_{hub}}^{1} I_x 2\pi r dr,$$
$$I_r(x)=\frac{1}{2}\mathrm{Re}\left(p\left(\partial\phi/\partial r\right)^*\right), W_{abs}=2\pi\int_{-L_M/2}^{+L_M/2} I_r dx, \quad (12)$$

where asterisks here denote complex conjugate. The sound powers for the incident, reflected, transmitted and absorbed are denoted by W_{in}, W_{ref}, W_{ex} and W_{abs}, respectively. Coefficients for sound absorption, α, reflection, β, are defined below together with the transmission loss (TL) and insertion loss (IL),

$$\alpha=W_{abs}/W_{in}, \quad \beta=W_{ref}/W_{in}, \quad TL=10\log_{10}\left(W_{in}/W_{ex}\right), \quad IL=10\log_{10}\left(W_{in}/\left(W_{ref}+W_{ex}\right)\right). \quad (13)$$

To examine the distribution of sound absorption along the absorber, the display of $I_r(x)$ alone can be misleading since the downstream portion has low values of $I_r(x)$ as sound is gradually absorbed. In other words, some sort of relative absorption ratio is more meaningful. We first use the actual overall transmission loss, TL, to define an equivalent attenuation rate L_r comparable to that defined for the infinite duct in Eq. (11), and use this to construct an equivalent local sound energy flux distribution against which $I_r(x)$ will be normalized and denoted as I_{r1},

$$L_r=TL/L_M, \quad I_{r1}(x)=I_r(x)\exp\left[\left(x-x_{LE}\right)L_r/\left(10\log_{10}e^1\right)\right], \quad (14)$$

where $x_{LE}=-L_M/2$ is the leading edge position of the absorber. The other quantity to be analyzed in a normalized manner is the amplitude of the sound expanded in terms of rigid-wall modes. The

normalization is based on the quadratic sum of the incident wave, and a decibel level is defined below,

$$SPL_n(x) = 10\log_{10}\left(\left|A_{mn}(x)\right|^2 \Big/ \sum_{k_{mn}\le k} \left|A_{mn}^{(in)}\right|^2 \right) \text{ dB}. \tag{15}$$

Optimization is now conducted for the total transmission loss (TL) using the cavity height $h_c(x)$ and MPP design parameters, including the aperture diameter d and porosity σ, while the panel thickness t_p is held as a constant for practical implementation convenience. For the examples given in this study, the dimensionless thickness is t_p=0.02, which corresponds to 1mm when $r_{tip}^* = 0.5\text{m}$. Chebyshev functions are used to construct a smooth distribution for each variable,

$$f_\mu(\bar{x}) = \sum_{n=0}^{\mu} a_n \cos\left(n\cos^{-1}\bar{x}\right), \bar{x} \in [-1,+1]. \tag{16}$$

A uniform property over the whole absorber corresponds to μ=0, and such a homogeneous absorber serves as a reference for studying the gain by a non-uniform absorber.

When a point source is launched at $r_s = 0.88$, the amplitudes of the five propagating modes are 0.61, 0.22, 0.43, 0.48 and 0.41, respectively, which is a fairly uniform spread of modes. Figure 3(a) displays the pressure contour with an insert for the normalized local sound absorption rate I_{r1}

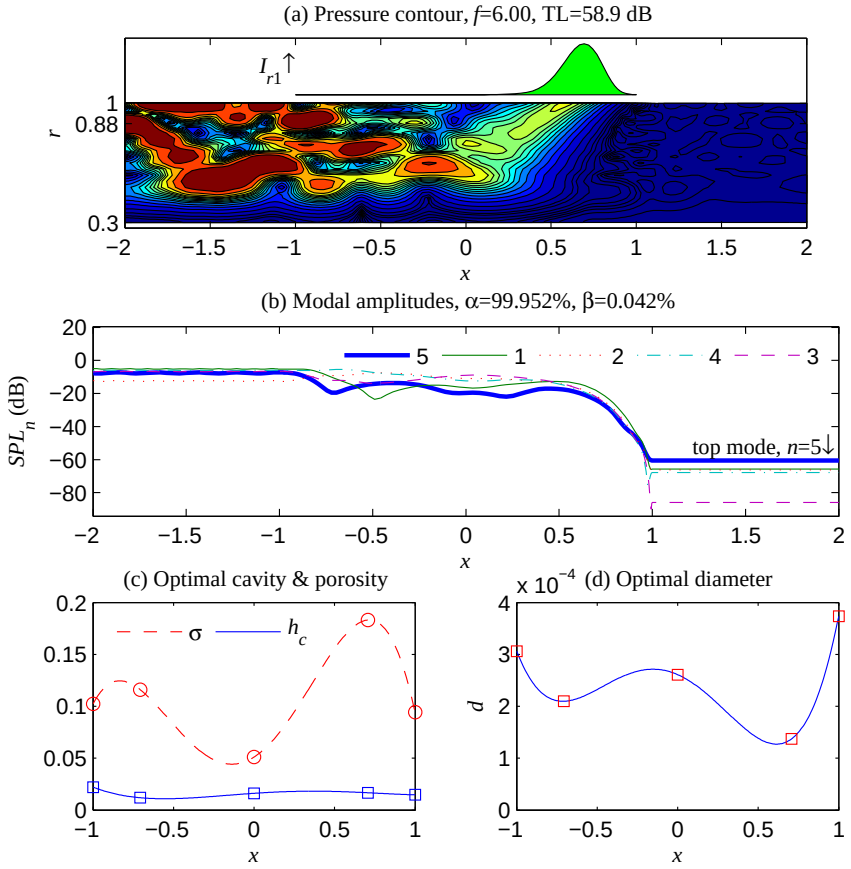

Figure 3: Almost complete absorption of all five propagating modes by a finite absorber with distributed impedance with the order of Chebyshev functions $\mu = 4$ optimized for a single frequency. The insert in sub-figure (a) and the sudden drop in modal amplitudes in (b) towards $x = 1$ show strong sound absorption towards the end of the absorber.

defined in Eq. (14). The overall absorber performance is written in the titles of sub-figures (a) and (b). High *TL* is achieved with negligible sound reflection. The insert in Figure 3(a) shows that the absorption mainly takes place near the downstream end of the absorber above the oblique pressure contour lines. Note that, if the absorber property is uniform, say using the best property shown in Figure 2(a), $h_c = 0.03, R = 2.15$, the local absorption curve $I_{r1}(x)$ would be rather uniform over the whole absorber length. Figure 3(b) shows the normalized modal amplitudes with sharp drop near the absorber trailing edge *x*=1. The exact mechanism needs further investigation but it surely has to do with the complex wave scattering caused by the impedance distribution. Figure 3(c) shows the distributions of the optimized cavity height (h_c, solid line) and MPP porosity (σ, dashed line) with five pivotal points marked along the curves. Figure 3(d) gives the distribution of optimized aperture diameter. Together, Figures 3(c) and 3(d) specify the distributed wall impedance design.

4. OPTIMIZATION FOR BROADBAND FREQUENCY

Having examined the performance of the absorber optimized for $f = 6$, it must be emphasized that such absorber is of little use for broadband noise. A new optimization is conducted to maximize the total sound absorption over a finite frequency band of $f \in [4.75, 7.5]$. The lower limit of 4.75 is so chosen that, according to Figure 2(d), the modes are not easily cut off by a uniform absorber. The higher limit of *f*=7.5 could be further extended but the essential features of results are expected to remain unchanged. Within this frequency band, the point source strength is assumed to be a constant. As the actual incident wave packet only contains the propagating modes, the high frequency sound has more energy content hence higher weighting in the optimization process. A

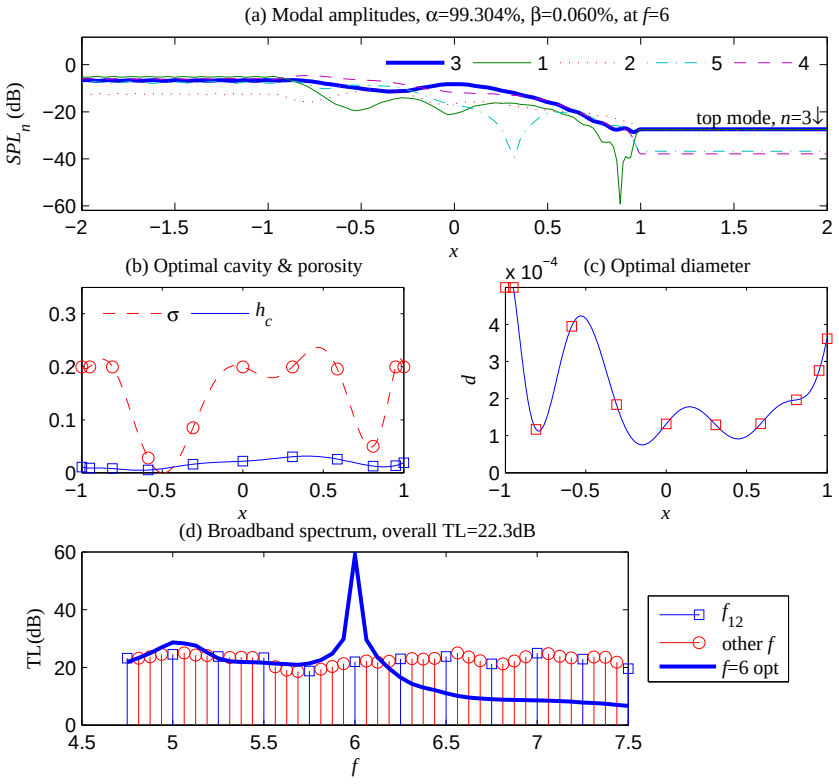

Figure 4: Broadband performance achieved by optimizing 10 segments of wall impedance consisting of MPP and cavity of various depth. (a) Modal absorption for the typical frequency of 6. (b) Optimized porosity σ and cavity depth h_c. (c) Optimized aperture diameter d. (d) TL spectra.

total of 12 discrete frequency points are chosen and denoted as f_{12},

$$f_{12} = 4.75, 5.0, 5.25, \cdots, 7.5\,. \tag{17}$$

Chebyshev expansion, Eq. (16), with order $\mu = 10$ is used to describe the wall properties. The broadband optimized result is shown in Figure 4. The energy-averaged *TL* is 21.9 dB. When the frequency interval of $\Delta f = 0.25$ is refined to $\Delta f/4$, similar spectral performance is obtained and the total *TL* actually increases to 22.3 dB. Such performance is more or less equivalent to the peak attenuation rate shown in Figure 2(a), $L_r = 10.43$ dB, which implies $TL = L_r L_M = 20.86$ dB. However, the peak in Figure 2(a) is obtained for the single frequency of $f = 6$. To make a fair comparison, a separate optimization is conducted for the same 12 frequency points using a uniform absorber (i.e., $\mu = 0$). The result is $TL = 13.3$ dB with the optimized parameters of

$$\sigma = 20\% \text{ (maximum specified)}, h_c = 1.966\times10^{-2}, d = 0.114\times10^{-3}\,.$$

In other words, the gain by the distributed absorber property is

$$\Delta TL = TL\big|_{\mu=10} - TL\big|_{\mu=0} = 21.9 - 13.4 = 8.5 \text{ dB}\,.$$

Compared with Figure 3(b), Figure 4(a) does not show a dramatic reduction of normalized modal coefficients, but it does still show a degree of enhancement of absorption towards the end of the absorber segment. Figure 4(b) shows the optimized cavity depth (h_c, solid line) and MPP porosity (σ, dashed line), while Figure 4(c) gives the aperture diameter *d*. Not much can be said about these distributions and an in-depth analysis is not expected to be easy. It is therefore necessary to check if these distributions are only useful for the 12 discrete frequencies, denoted earlier as f_{12} in Eq. (17), used in the optimization. Figure 4(c) shows the TL spectrum with f_{12} shown in open-square stem plot. Three more frequencies calculated within each frequency interval are shown in open circles. These do not deviate from the pattern of TL for f_{12}. The conclusion is that the optimized wall impedance works for a broad frequency band. When the design optimized for *f*=6, which is shown in Figures 3(c) and 3(d), is used to calculate for the broadband, the result is shown in solid line in Figure 4(d). This is a resonance-like behaviour in the sense that the good performance at *f*=6 does not carry over to other frequencies especially the higher frequencies.

The second check of whether the optimized design is peculiar to some frequency or source characteristics is carried out by varying the circumferential mode *m* with results shown in Figure 5.

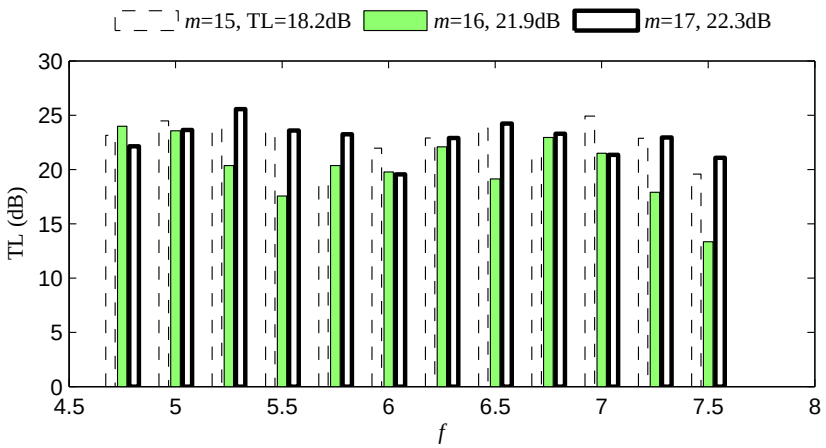

Figure 5: Comparison of performance for 3 circumferential modes using the MPP optimized for mode m=16.

Using the same design shown in Figures 4(b) and 4(c), the absorption for the two neighbouring modes, m=15 and 17, is calculated and the results are presented in Figure 5 in a grouped bar chart. The energy-averaged transmission losses for the three modes of 15, 16 and 17 are, respectively, 18.2, 21.9, 22.3 dB. The fact that the result for m=16 is naturally sandwiched between the two other modes implies that the broadband design is not peculiar to one source character in a way like resonators are for their resonance frequencies. The fact that the performance for m=15 is worse than m=16 is expected since lower order modes are known to be more difficult than higher order modes.

5. CONCLUSIONS

The numerical simulations presented here are a starting point in the search for improved passive control of complex duct noise. The following preliminary conclusions can be drawn.

1. An impedance wall can be optimized for absorbing a pure tone with uniform wall properties. Typically, the optimal local resistance should be increased for higher frequencies. However, the optimal performance deteriorates with frequency. When an axial distribution of wall properties is considered, significantly better sound absorption may be achieved. In the example given, the bulk sound absorption takes place near the downstream edge of the absorber.
2. When optimization is applied to a broad frequency band, using a microperforated panel with cavity of various depth, it is shown that improved performance can be obtained for the difficult regime of high frequencies. The overall absorber performance is much improved from the optimal uniform absorber. The optimized wall property distribution shows interesting undulations for which more work is required to examine the exact working mechanisms.
3. The optimal performance obtained for a set of discrete frequencies in a finite frequency band remains to be good for all frequencies in the band. Similar conclusions are achieved for different circumferential modes although noise of lower modal index is in general more difficult to attenuate.

ACKNOWLEDGEMENT

The work is supported by a Major Fundamental Research (973) Scheme of China (project code 2012CB7202).

BIBLIOGRAPHY

[1] W. K. Blake – *Mechanics of flow-induced sound and vibration*. Academic Press, Orlando, Fla., **1986**.

[2] J. P. Boyd – *Chebyshev and Fourier spectral methods*. 2nd ed., Dover, New York, **2001**.

[3] L. Huang – *Membrane covered duct lining for high frequency noise attenuation – prediction using a Chebyshev collocation method*. J. Acoust. Soc. Am. 124, 2918-2929, **2008**.

[4] H. H. Hubbard – *Aeroacoustics of flight vehicles- theory and practice*, *volume I noise sources*. Acoustical Society of America, New York, **1995**.

[5] J. B. Keller, D. Givoli – *Exact non-reflecting boundary conditions*. J. Comp. Phy. 82, 172-192, **1989**.

[6] D.-Y. Maa – *Potential of microperforated panel absorber*. J. Acoust. Soc. Am. 104, 2861-2866, **1992**.

[7] M. L. Munjal, A. G. Galaitsis, I. L. Ver – *Passive Silencers*. In Noise and Vibration Control

Engineering: Principles and Applications, 2nd ed, Chapt 9, edited by I. L. Ver and L. L. Beranek, Wiley, New Jersey, **2006**.

[8] L. Nauhaus, J. Schulz, W. Neise, M. Moser – *Active control of the aerodynamic performance and tonal noise of axial trubomachines*. Proc. Inst. Mech. Eng. 217, 375-383, **2003**.

[9] S. W. Rienstra, W. Eversman – *A numerical comparison between the multiple-scales and finite-element solution for sound propagation in lined ducts*. J. Fluid Mech. 437, 367-384, **2001**.

[10] I. Singer, E. Turkel – *A perfectly matched layer for the Helmholtz equation in a semi-infinite strip*. J. Comp. Phy. 201, 439-465, **2004**.

[11] X. F. Sun, X. Y. Wang, L. Du, X. D. Jing – *A new model for the prediction of turbofan noise with the effect of locally and non-locally reacting liners*. J. Sound Vib. 316, 50-68, **2008**.

[12] R. H. Thomas, R. A. Burdisso, C. R. Fuller, W. F. O'Brien – *Active control of fan noise from a turbofan engine*. AIAA J. 32, 23-30, **1994**.

[13] J. M. Tyler, T. G. Sofrin – *Axial flow compressor noise studies*. SAE Trans. 70, 309-332, **1962**.

© Dr Lixi Huang